FREE-STANDING CARBON TARGETS FOR ENHANCED CARBON ION ACCELERATION WITH PETAWATT CLASS LASERS

Laurențiu DINCĂ[1,2], Cosmin JALBĂ[1,2], Bogdan DIACONESCU[3], Bogdana MITU[4]

The advent of new PetaWatt (PW) class laser facilities create opportunities for laser induced plasma ion acceleration studies where the dynamics and effects of laser target interaction are intimately linked to target structure. In the case of 1 to 10 PW lasers like the ones at ELI-NP, nanometer-thin solid targets can be used to generate high-density and high-energy ion beams via relativistically induced target transparency or radiation pressure acceleration mechanisms. In preparation for experiments at PW laser facilities, we have developed an accessible and high throughput method for fabricating and characterizing nanometer thin free-standing and millimeter lateral size diamond-like carbon targets.

Keywords: Free-standing film; Carbon target; High-power laser acceleration; Plasma enhanced chemical vapor deposition.

1. Introduction

The nanometer-thin targets undoubtedly enrich the laser-driven acceleration mechanisms by accessing laser induced plasma acceleration regimes like relativistically induced target transparency (RIT) [1], breakout afterburner (BOA) [2] and radiation pressure acceleration (RPA) [3], thus enhancing the ion's kinetic energy and flux density than what thicker targets would allow [4]. Within this context, laser light intensities $I \geq 10^{18}$ W/cm^2 are required, as expected when using 1 and 10 PW beams at ELI-NP facility. As a matter of fact, the estimations [2] for 1 PW ELI-NP beams give an optimal target thickness for radiation pressure acceleration regime (BOA/RPA) around 100-150 nm, while for 10 PW ELI-NP beams is around 15-20 nm. To reach the ion energies of tens of MeV/u with ultrashort pulses at $I\lambda^2 > 10^{20}$ W·cm^{-2}·μm^2 and contrast at least as good as 10^{-8} can require sub-micrometer targets involving the (relativistically induced) target

[1] PhD student, SDIALA, National University of Science and Technology POLITEHNICA BUCHAREST (UNSTPB), Bucharest, Romania
[2] Doctoral research assistant, ELI-NP, HORIA HULUBEI National Institute for R&D in Physics and Nuclear Engineering (IFIN-HH), Măgurele, Romania,
e-mail: laurentiu.dinca@eli-np.ro, cosmin.jalba@eli-np.ro
[3] Senior research scientist 2nd degree, ELI-NP, HORIA HULUBEI National Institute for R&D in Physics and Nuclear Engineering (IFIN-HH), Măgurele, Romania,
e-mail: bogdan.diaconescu@eli-np.ro
[4] Senior research scientist 1st degree, National Institute for R&D in Laser, Plasma and Radiation Physics (INFLPR), Măgurele, Romania, e-mail: mitu.bogdana@inflpr.ro

normal sheath acceleration (BOA/TNSA) [2, 5], with which our experimental data agree. Moreover, the flat targets need to have the front side roughness on the order of λ/10 on zones compared with the focus spot size which for ~F/3 f-number at ELI-NP optics corresponds to less than 3 μm spot diameter. This constraint assures the prevalence of specular propagation through the solid diamond-like carbon (DLC) film when the incidence starts, due to a good compliance with Rayleigh roughness criterion [6]. Thus, the focus spot is less randomly scattered by the front surface at that moment, and the laser pulse pedestal energy transfer to preplasma formation starts in a more contoured boundary inside the target. In such condition, the conversion of solid film to preplasma will be more effective, so an ion bunch will be emitted at higher energy and flow after the subsequent interaction of the main laser pulse with preplasma. Furthermore, since we need to focalize the entire laser energy on the target itself which also needs mechanical support, an apertured substrate is required for it. Therefore, the target film must be self-supported (free-standing) on the substrate. To avoid the energy transfer from high power laser pulse to the lateral substrate of free-standing opening, the lateral stretches' size of millimeters is mandatory.

Because of high film surface-to-bulk ratio, the shear and breakage hazards may occur during manipulation, so the target material requires a high mechanical strength.

In our work, the goal is to implement a thin carbon target manufacturing method for high-power laser (HPL) experiments, the aspects regarding the laser-target interaction being treated here as much as necessary to investigate the matching of target properties to this application. Morphological and chemical characterizations were performed to establish the target quality compliance for PW class laser acceleration experiments, in order to use in the 1 PW commissioning experiment within ELI-NP.

2. Materials and methods

Our contribution to a carbon/proton (the later from adsorbed water films at 10^{-6} mBar vacuum level) laser-driven acceleration experiment has been to provide free-standing DLC films, a specific class of materials that can meet the above requirements, particularly the mechanical strength and also provide energetic ion-beams bio-compatible for future hadron therapy studies.

The target surface should be sufficiently smooth on the front side, which is achieved by machine polishing the copper substrates on the deposition side prior to DLC growth, operation described below:

- cutting, flatting, polyvinyl alcohol (PVA) gluing the copper substrates on an aluminum puck (polishing holder);
- thermal drying of PVA at 90°C for 2 h 30 min;

- removal of dry PVA in excess on the puck between copper substrates using sandpaper and a slightly moist wipe;
- drying at 90°C for 30 min;
- polishing (30 min/20 rpm/45-50 torque) using diamond abrasive solution (6 μm granulation);
- polishing (30 min/50 rpm/38-40 torque) using the same abrasive solution;
- lateral covering of high-polished substrates with adhesive tape and fully covering of low-polished substrates;
- polymeric film spraying on the top of the puck to mask the copper portions uncovered by adhesive tape, conferring the protection of the surface until DLC film deposition;
- removal of adhesive tape and thermal curing of the polymeric film at 90°C for 30 min using an increasing ramp of 30 min;
- detaching the polished copper substrates from the puck after immersion in water heated to 40°C for 2÷3 h, natural drying of substrates, and preparation for the deposition process using the following steps:
- removal of the polymeric protective layer in acetone bath;
- removal of PVA traces by ultrasonic cleaning in ultrapure water (40 °C, 30 min);
- alcohol rinse and natural drying.

DLC films were grown on the polished side of copper substrates by plasma-enhanced chemical vapor deposition (PECVD) using an H-enriched hydrocarbon gas mixture [7], a total pressure of ~10^{-3} mbar, and a high-frequency electrical signal of 13.56 MHz and 100 watts. After DLC deposition, the copper substrates were etched to obtain the patterned free-standing DLC films. The patterning has is described below, avoiding ambient light photoresist activation until corrosion step:

- positive photoresist spraying on DLC/Cu sample and thermal curing at 90°C for both sides;
- UV-mask mounting on DLC/Cu sample (holes pattern on substrate side and complete obturation on DLC side);
- UV exposure in 4 positions for uniformity (4÷16 min total);
- developing in sol. NaOH 10 g/l (2÷10 min);
- corrosion of copper (40÷90 min) in 40% iron (III) chloride;
- careful rinses in water, in acetone (photoresist removal), and natural drying.

The photoresist uniformity and thickness play an important role in the required time of each patterning step, and the exposure and developing quality also experience those influence. The patterned DLC/Cu samples were cut and glued on the aluminum matrix frames, in order to use the DLC film targets in laser-driven acceleration.

3. Results and discussion

The optical microscopy (Fig. 1) and profilometry (Fig. 2) have revealed the morphology and roughness on the free-standing DLC front side. The energy-dispersive X-ray spectrometry (EDX) performed within scanning electron microscopy (SEM) has determined the chemical element composition of DLC film front side (Fig. 3, 4).

Generally, the substrate holes are slightly larger on the substrate external surface than on the substrate-film interface due to the chemical corrosion isotropy, the substrate material being etched at same rate on all directions. The free-standing DLC film wrinkles can be attributed either to the thermal expansion coefficient difference between the copper and DLC which manifests during the PECVD process when both materials are heated at over laboratory temperature, or to the self-supported DLC film mechanical deformation during the photoresist film removal in the acetone bath. The target film wrinkles don't alter the normal incidence set-up, since these are much larger than spot size and the beam is locally perpendicular to the target. Instead of, in a plasma mirror such wrinkles modify the HPL wavefront which can thus defocus on target and diminish or prevent the acceleration process. On the plasma mirror free-standing having lateral stretch larger than of targets, more flatness avoids this trouble, and the requirement to document the wrinkling occurrence is critically in order to avoid or compensate it.

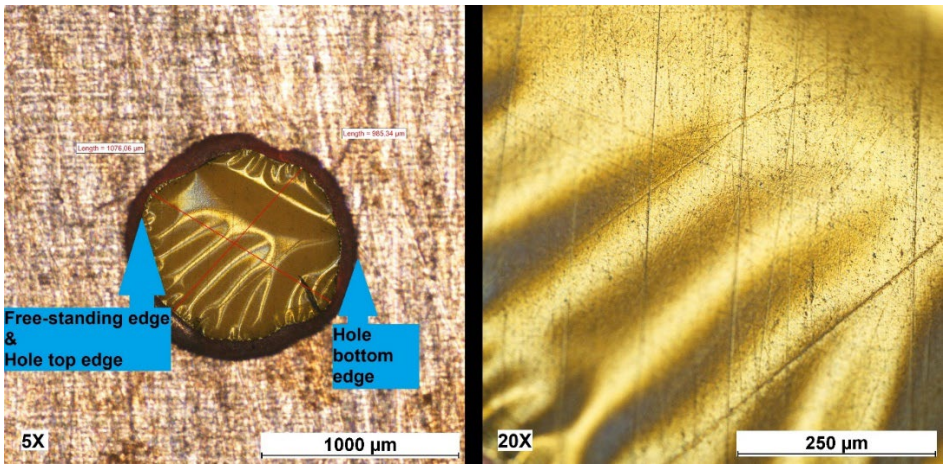

Fig. 1. Optical images (5X, 20X) of free-standing DLC film on Cu substrate (front side): substrate-hole and free-standing zone (980÷1080 µm size)

The Rayleigh roughness criterion at normal incidence statutes the Rayleigh roughness parameter [6] in reflection (Ra_r) must be lower than 0.8 in order to consider the surface is enough smooth to prevail the coherent component of the reflected electromagnetic wave [8]. The criterion is also extended when the same optical interface is passed, but a similar parameter (Ra_t) is used in transmission with

the upper limit of Ra_r [6]. This extension is here in concerning because the light is absorbed along the transmission paths in film and the preplasma formation is sustained by absorption. Minimizing the diffused transmission, the absorption is more spatially contoured. The Ra_t depends on the roughness [6] as in Eq. 1 when the vacuum is considered the front optical medium and the R_q is expressed as λ/p with the reduction factor p, where n(λ) is the PECVD-grown DLC refractive index which is considered in 1.57÷2.32 interval at a wavelength in the middle of visible range [9].

$$p = \frac{\pi|1 - \mathrm{n}(\lambda)|}{\mathrm{Ra_t}} \tag{1}$$

We have established an upper limit of λ/10 for roughness R_q in order to satisfactory compliance the Rayleigh criterion at normal incidence for both transmission (λ/5.3÷λ/2.3 resulting from Eq. 1 for DLC) and reflection (λ/8 [8]). The latest case is regarded to furtherly transfer the fabrication method on sacrificial plasma mirrors, and the considered R_q upper limit is more restrictive in comparison with the limit only required in transmission for this reason.

The optical profilometry data confirm the upper limit of λ/10=81 nm (λ=810 nm for ELI-NP HPL pulses [10]) of free-standing DLC film roughness for 75% (more than half) of determined R_q roughness values, which is high-lighted by the acquired line profiles of 30 μm length that are 31 times larger than the diffraction limit of HPL spot (1.2λ=972 nm). The mean determined values of line profiles after linear tilt correction (Tab. 1) is 78.5 nm with standard deviation of 22.7 nm.

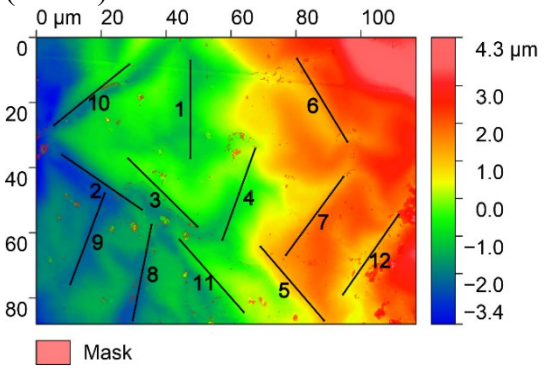

Fig. 2. Optical 3D profilogram and 12 line-profiles on free-standing DLC (53.6 nm film thickness)

Table 1

Roughness values of line-profiles

Profile no.	**1**	**2**	**3**	**4**	**5**	**6**
R_q [nm]	72.0	63.4	69.0	139.9	89.5	64.5
Profile no.	**7**	**8**	**9**	**10**	**11**	**12**
R_q [nm]	54.1	75.5	62.9	97.0	73.5	81.0

EDX and SEM on the front side of self-sustaining DLC film show that copper and iron impurities remain at very low atomic concentrations

(1.14%±0.13% Fe; 0.78%±0.09% Cu) after iron chloride etching. The traces of Fe come from etchant solution and the Cu from an uncomplete etching of substrate. The oxygen peak shows a content of 21.56%±0.76%, the element being present in the traces of the metal oxides and photoresist impurities of film rear side (opposite to the front side). The oxygen content could be partially attributed to the DLC film itself, depending on the carbon content derived from photoresist. The total carbon content is 76.52%±1.83% from the DLC film and probably from the photoresist impurities.

The iron concentration could be corelated to a very low quantity of carbon, while the Fe-C alloy phase diagram would allow the Fe-containing microparticles to form such chemical structures at the room temperatures which are involved during and after etching process. Such Fe-C structures are promoted to form in small quantities on carbon surface by iron-chloride solution, not dissolvable in aqueous medium and rinse solvents, so their presence after entire patterning chain weakly influence the EDX spectra.

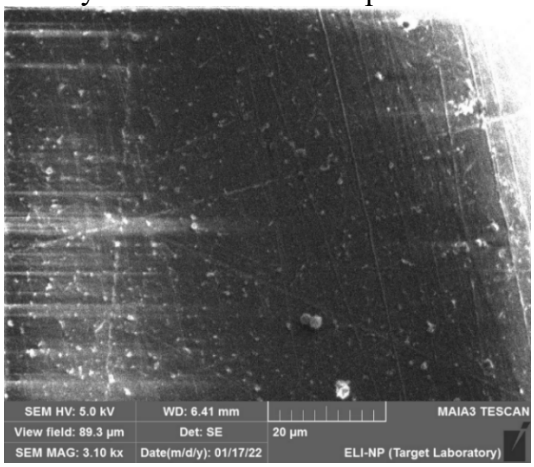

Fig. 3. SEM picture on free-standing DLC film (front side)

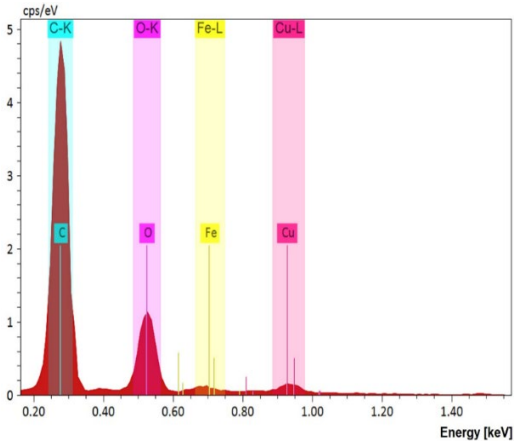

Fig. 4. EDX spectra on free-standing DLC film (front side)

The target normal sheath acceleration (TNSA) is widely encountered mechanism because of more accessible conditions of occurrence regarding the target thicknesses and the pulse contrasts and intensities [11-13], reaching the ion energies and flows needed for most applications [14]. In this regime, when the HPL pedestal/prepulse is incident the full ionization of solid target atoms occurs leading to a preplasma. When the main pulse interacts, a hot electron jet which generates a strong charge separation electric field in the plasma appears on the front-rear direction. An energetic and dense ion bunch is emitted towards laser propagation direction because of the electric field [12 ,15]. The high charge to mass ratio ions gain the most part of energy, such as hydrogen and carbon that the DLC target contains [16]. The accelerated hydrogen ions (protons) originate from the rear

surface impurities which consist of H_2O and C_xH_y compounds adsorbed from the air or left on the surface after target manufacturing. The carbon component of the ion flow prevalently originates from the DLC, the surface hydrocarbon impurities giving a less contribution.

The DLC targets prepared by us have been used in the 1 PW commissioning campaign within the E5 experimental area of ELI-NP, producing energetic ions in TNSA regime [17]. The accelerated carbon ions and protons have reached cut-off kinetic energies of ~180 MeV and ~38 MeV (Fig. 5) using a HPL pulse of 19 J before plasma mirror, which was incident on a 380 nm free-standing DLC film target grown on Cu substrate [17]. Despite the iron and copper traces were found on the target surface, such ions were not detected in ion bunch especially due to its placing on the front side of a not so thin target (~0.4 μm) where the ion acceleration mechanism has occurred in the rear part. Anymore, the higher weights of Fe and Cu ions would mitigate the kinetic energy gain.

4. Conclusions

We have developed an accessible and high throughput method for nanometer thin, millimeter sized aperture and free-standing DLC target fabrication to be used in high-power laser experiments. A free-standing lateral extent of the order of millimeters was found by optical microscopy, while the optical profilometry has proved the laser-driven acceleration compliance of DLC films in terms of λ/10 limit on zones compared to focal spot size. The EDX analysis has confirmed a low-level contamination on the free-standing DLC film front side in context of TNSA occurrence.

5. Acknowledgements

The SEM/EDX analysis and the copper substrate polishing were performed with the help of Ph.D. Cristina Gheorghiu and Tech. Daniel Popa at ELI-NP Target Laboratory. The PECVD DLC growth was made with the help of Ph.D. Bogdana Mitu and her team at INFLPR.

This research was supported by IFIN-HH within the framework of the ELI-NP project - phase II (co-financed by the Romanian Government and the European Union through the European Regional Development Fund – the Competitiveness Operational Program, grant no. 1/07.07.2016, COP, ID 1334).

R E F E R E N C E S

[1]. *J. C. Fernández*, *D. C. Gautier*, *C. Huang*, *S. Palaniyappan*, *B. J. Albright*, *W. Bang*, *et al.*, Laser-plasmas in the relativistic-transparency regime: science and applications, Physics of Plasmas 24 (2017) 056702. https://doi.org/10.1063/1.4983991.

[2]. *D. Sangwan*, *O. Culfa*, *C. P. Ridgers*, *S. Aogaki*, *D. Stutman*, *B. Diaconescu*, Simulations of carbon ion acceleration by 10 PW laser pulses on ELI-NP, Laser and Particle Beams 37 Issue 4 (2019) 346-353. https://doi.org/10.1017/S0263034619000648.

[3]. *L. C. Stockhausen*, *R. Torres*, *E. C. Jarque*, Simulations of radiation pressure ion acceleration with the VEGA Petawatt laser, Nuclear Instruments and Methods in Physics Research Section A: Accelerators, Spectrometers, Detectors and Associated Equipment 830 (2016) 550-555. https://doi.org/10.1016/j.nima.2015.10.068.

[4]. *J. Badziak*, Laser-driven ion acceleration: methods, challenges and prospects, Journal of Physics: Conf. Series 959 (2018) 012001. https://doi.org/10.1088/1742-6596/959/1/012001.

[5]. *A. Magureanu, L. Dinca, C. Jalba, R. F. Andrei, I. Burducea, D. G. Ghita, V. Nastasa, M. Gugiu, T. Asavei, O. Budriga, D. Ticos, V. Craciun, B. Diaconescu, C. M. Ticos,* Target characteristics used in laser-plasma acceleration of protons based on the TNSA mechanism, Frontiers in Physics, Sec. Interdisciplinary Physics (2022) 10:727718. https://doi.org/10.3389/fphy.2022.727718.

[6]. *N. Pinel*, *C. Bourlier*, *J. Saillard*, Degree of roughness of rough layers: extensions of the Rayleigh roughness criterion and some applications, Progress in Electromagnetics Research B 19 (2010) 41-63. http://dx.doi.org/10.2528/PIERB09110907.

[7]. *P. K. Bachmann*, *D. Leers*, *H. Lydtin*, Towards a general concept of diamond chemical vapour deposition, Diamond and Related Materials 1 Issue 1 (1991) 1-12. https://doi.org/10.1016/0925-9635(91)90005-U.

[8]. *F. T. Ulaby*, *D. G. Long*, Microwave radar and radiometric remote sensing, Chapter 10: Surface Scattering Models and Land Observations (2013) University of Michigan Press, ISBN-13: 9780472119356.

[9]. *M. Hiratsuka*, *H. Nakamori*, *Y. Kogo*, *M. Sakurai*, *N. Ohtake*, *H. Saitoh*, Correlation between optical properties and hardness of diamond-like carbon films, Journal of Solid Mechanics and Materials Engineering 7 (2013) 187-198. https://doi.org/10.1299/jmmp.7.187.

[10]. *M. O. Cernăianu*, *P. V. Ghenuche*, *et al.*, Commissioning of the 1 PW experimental area with an experiment on TNSA ion acceleration, ELI-NP Annual Report 2020-2021 (2022) 91-93. https://www.eli-np.ro/documents/ELI-NP-Annual_Report-2020-2021.pdf.

[11]. *S. Fourmaux*, *S. Buffechoux*, *B. Albertazzi*, *D. Capelli*, *A. Lévy*, *S. Gnedyuk*, *L. Lecherbourg*, *et al.*, Investigation of laser-driven proton acceleration using ultra-short, ultra-intense laser pulses, Physics of Plasmas 20 (2013) 013110. http://dx.doi.org/10.1063/1.4789748.

[12]. *S. S. Bulanov*, *Q. Ji, S. Steinke*, *T. Schenkel*, *E. Esarey*, *W. P. Leemans*, Advanced acceleration mechanisms for laser driven ions by PW-lasers, Proceedings of IPAC2016, Busan, Korea (2016) 2082-2084, ISBN 978-3-95450-147-2.

[13]. *J. H. Bin*, *M. Yeung*, *Z. Gong*, *H. Y. Wang*, *C. Kreuzer*, *M. L. Zhou*, *M. J. V. Streeter*, *P. S. Foster*, *et al.*, Enhanced laser-driven ion acceleration by superponderomotive electrons generated from near-critical-density plasma, Physical Review Letters 120 (2018) 074801. https://doi.org/10.1103/PhysRevLett.120.074801.

[14]. *J. Badziak*, Laser-driven ion acceleration: methods, challenges and prospects, Journal of Physics: Conference Series 959, PLASMA-2017, Warsaw, Poland (2017) 012001. https://doi.org/10.1088/1742-6596/959/1/012001.

[15]. *S. C. Wilks*, *A. B. Langdon*, *et al.*, Energetic proton generation in ultra-intense laser–solid interactions, Physics of Plasmas 8 (2001) 542–549. https://doi.org/10.1063/1.1333697.

[16]. *A. Higginson*, *R. J. Gray*, *M. King*, *R. J. Dance*, *S. D. R. Williamson*, *N. M. H. Butler*, *R. Wilson*, *R. Capdessus*, *C. Armstrong*, *J. S. Green*, *S. J. Hawkes*, *P. Martin*, *W. Q. Wei*, Near-100 MeV protons via a laser-driven transparency-enhanced hybrid acceleration scheme, Nature Communications 9 (2018) 724. https://doi.org/10.1038/s41467-018-03063-9.

[17]. *** ELI-NP webpage (Nov. 24th, 2021). https://www.eli-np.ro/article.php?id=29.